Journal of Colloid and Interface Science 544 (2019) 172–177

Contents lists available at ScienceDirect

Journal of Colloid and Interface Science

journal homepage: www.elsevier.com/locate/jcis

Regular Article

The locally columnar model for clay/polymer systems: Connections to scattering experiments

Henrich Frielinghaus [a,*], Kerstin Koch [a], Viviane Pecanha Antonio [a], Yohei Noda [b], Satoshi Koizumi [b]

[a] Jülich Center for Neutron Science at MLZ, Forschungszentrum Jülich GmbH, Lichtenbergstrasse 1, 85747 Garching, Germany
[b] Institute of Quantum Beam Science, Ibaraki University, 162-1, Shirakata, Ibaraki 319-1106, Japan

GRAPHICAL ABSTRACT

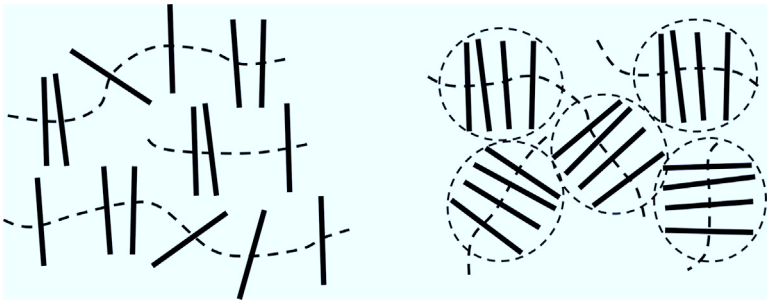

ARTICLE INFO

Article history:
Received 28 January 2019
Revised 26 February 2019
Accepted 27 February 2019
Available online 28 February 2019

Keywords:
Clay
Polymer
Nanocomposite
Scattering model
Thermodynamic model

ABSTRACT

A tight connection of scattering to thermodynamic models is missing for clay systems. A new approach called "*locally columnar model*" gives an attempt for making this connection. The scattering model assumes an up-lining of clay particles with strong paracrystalline order and refers to a chemical potential/distance dependence. The thermodynamic model assumes a bidisperse distance distribution and gives input to the scattering model. Experimentally, polymer/clay systems with many molecular polymer masses were studied showing all very similar scattering curves. While the dominating bulk phase shows only the same weak tendency to stack formation for all molecular polymer masses, one coexisting phase with stronger stack formation was identified. The latter sample was used to determine the thickness of the clay platelets with adsorbed polymer that was then used to model the dominating bulk phase. The comparisons to the theory revealed that (a) most polymers are tightly bound to the clay, and (b) an agreement between the modeling and the theory was achieved. The main result of the experiments is the fraction of free polymers of 1:2400 that are not tightly bound to the clay particles.

1. Introduction

Clay/polymer nanocomposites provide many advantages for the application [1] ranging from fire retardancy, over inhibition of small molecule diffusion to enhanced mechanical strength and scratch resistance. All of this benefits from the large aspect ratio of the clay platelets. Urgently, comparisons between the structure and thermodynamic models are needed to allow for directed optimizations of the application. Scattering experiments provide very good structural characterization [2–5], especially if the clay platelets are regularly ordered. These experiments then provide a feedback to the formulations of industrial applications.

Many thermodynamic models for clay systems exist ranging from rather analytical approaches [6] over density functional theory [7–10] to simulations [11]. Similarly, for spherical colloids

* Corresponding author.
E-mail address: h.frielinghaus@fz-juelich.de (H. Frielinghaus).

https://doi.org/10.1016/j.jcis.2019.02.091
0021-9797/

thermodynamic models exist [12]. Also attempts to connections to scattering models have been made [13]. All in all these approaches stay at a rather rudimentary level. Here, scattering experiments can give very good insight to the structure of the nanocomposite and allow for quantitative comparisons with models.

We developed a scattering model that deals with a one-dimensional paracrystalline [14,15] order connecting the distance distribution to a chemical potential/distance dependence. The thermodynamic model assumes a bidisperse distance distribution and provides this missing input to the scattering theory. Scattering experiments with many molecular polymer masses were conducted using x-rays and neutrons. Thermodynamic equilibrium was assumed by tempering the samples at 100 °C followed by a quench to room temperature where the system freezes due to partial polymer crystallization. Finally, the model and the experiments are compared.

2. Materials and methods

The clay particles were obtained from Süd Chemie (Rockwood), now belonging to the BYK chemicals group. The Laponite RD (LRD) is reported to have a diameter of 250 Å and a thickness of 10 Å. The Laponite material was used without further cleaning. Polyethylene oxide was purchased from Sigma Aldrich with molar masses of 600, 1000, 1500, 3350, 10,000, 20,000 and 100,000 g/mol. All polymers were used without further cleaning. The nanocomposites were prepared from solution at concentrations of 4.35%wt clay and 8.70%wt polymer in 87%wt water. After stirring for several hours, the solutions were first dried to approx. 50% dry mass in a rotor vap and then further dried in high vacuum. After the nanocomposite appeared dry the sample was tempered at 100 °C under high vacuum. We assume that the dispersion reaches equilibrium at these high temperatures, and the quick quenching to room temperature with the unavoidable crystallization does only freeze the clay particle arrangement. Assuming a clay density of 2.6 g/cm^3, the polymer concentration is φ_{pol} = 84%vol.

X-ray diffraction has been carried out on a Bruker D2 Phaser instrument with a copper Kα source (30 kV, 10 mA, λ = 1.541 Å). The incident beam was collimated to 0.1° divergence. The sample was placed on a silicon waver as a powder (or as highly viscous pieces cut from the whole specimen). The beam stop was placed at a distance of 3 mm. The 2θ angle was scanned with a single detector with a precision of 0.02°. The shading characteristics of the beam stop from the rather flat scattering of the sample with the lowest molar mass have been used to correct the scattering at smallest angles.

SANS/WANS were conducted at the instrument iMATERIA at J-PARC, Tokai, Japan that was supported by the team of the Ibaraki University. The neutron source is a pulsed source. The neutron wavelength band was 1–10 Å, and the small angle and wide-angle detectors were used. Instrumental details and data reduction processes are described in Refs. [16,17].

Model. For clay polymer systems the authors developed a structure factor [1] that describes a strong paracrystal. The basic idea behind is that locally the clay particles line up concentrically to form stacks with varying spaces between. These concentric stacks experience a very high entropic violation of $Nk_B\ln(2)$ when interdigitating over an approaching distance connected to the fuzziness of the stacks. Thus, we believe that preferentially the platelets line up along slightly curved lines without interdigitations. The polymers experience a chemical potential difference $\Delta\mu_p$ between the platelets, and the next neighbor distribution is an exponentially decaying function $\Psi(\Delta) \sim \exp(-\Delta/L)$ as a function of the distance Δ with a typical decay length L, whereas the shortest distance is described by the parameter d that arises from the platelet thickness. The resulting structure factor is written as:

$$S(q) = \frac{(qL)^2}{2 + (qL)^2 - 2\cos qd + 2qL\sin qd} \quad (1)$$

In Ref. [1] the decay length L is connected to the purely entropic chemical potential $\Delta\mu_p$, which for strongly 1-dimensional confined polymers is approximately $\mu = k_BT\,(1 - \Delta^2/R_{ee}^2) \approx k_BT$ with Δ being the confinement space and R_{ee} the polymer end-to-end distance. The resulting overall chemical potential for the material in between the platelets is defined by the number of confined polymers n according to $n = \pi R^2\Delta/V_m$ with R being the platelet radius and V_m being the polymer molecular volume (in this sense, the scattering model considers the total thermodynamic potential nμ (i.e. the Gibbs free energy) of all polymers between two neighboring platelets in the sense of the grand canonical ensemble (i.e. with the coexistence of infinite free polymer, so the rare case of large distances Δ > L could occur)). So the decay length results in:

$$L = \frac{V_m}{\pi R^2 \Delta\mu_p/k_BT} \approx \frac{V_m}{\pi R^2} =: L_0 \quad (2)$$

This means that the polymers are in contact with a surrounding space that provides enough polymers in a melt state for a free exchange. From that model, an average number $\langle N\rangle$ of nearest clay particles, i.e. an effective stack number, could be derived:

$$\langle N\rangle \approx \sqrt{\frac{3}{\pi^2}\cdot\frac{d^2}{L^2} + 1} \quad (3)$$

This definition of an effective stack results from the peak width, i.e. the correlation length, of the platelet scattering. As we have discussed, large distances Δ > L may occur, but they do not contribute to the definition of the effective stack number. Practically, the molar volumes of polymers are quite small that bare predictions from that simple model results in small L and thus in large stack numbers, i.e. kind of a phase separation. The background is that a rather large reservoir of free polymers was assumed that coincides with low clay concentrations (i.e. the assumption was the grand canonical ensemble). In experiments and the real applications the concentrations of clay particles are moderate to rather high, such that the coexisting polymer reservoir is finite. Apart from that, there are quite strong attractive interactions between the polymer and the platelets. Following the blob concept [18] where tight crosslinks or strong binding causes the subunits (or loops) of the polymer to appear as independent sources of entropy, the molar masses of the subunits (or loops) are not dependent on the whole polymer mass anymore. Thus, the dominating entropic contributions of the confined polymer are not dependent on the distance anymore. This means, that other sources of entropy have to be considered now. Apart from that, we assume that a very small fraction of not-bound polymers still exist that still introduce a confinement entropy as discussed above. The latter condition means that the parameter L_0 is considerably larger.

In this manuscript, a more detailed entropy for the clay distances and a polymer configurational entropy will be derived that then feeds back into an average stack number N and finally an effective decay length L. While the classical polymer configurational entropy is conceptually described by the abovementioned formulae, the additional entropy focuses on the degree of freedom of the platelets. Here, it is assumed that the orientational degree of freedom is dominating this additional entropy. The platelets are considered to line up concentrically, and thus the neighbor platelet to the first platelet (being perpendicular to the line) can cover a solid angle of $4\pi\sin(\vartheta) = 4\pi\,\Delta_1/R$ with Δ_1 being the average platelet distance in the stack that gives the sine of the maximum tilt

angle ϑ assuming concentric platelets. Consequently the full stack can freely rotate with a full solid angle of $4\pi\Delta_2/R$ with $\Delta_2(N) = N\delta-(N-1)\Delta_1$ with δ being the *average* space for the platelet in a moderately concentrated system. Again, Δ_2 makes the connection of the stack spacing with the maximum tilt angle of the whole stack. The two distinct cases of the platelet distance within the stack Δ_1 and the stack distance Δ_2 highlight the bidisperse character of this model. In principle, the solid angle cannot exceed 4π, and therefore the value levels off at larger dilution. Within our manuscript, we don't need to consider this situation. The purely entropic Gibbs free energy per clay platelet reads now:

$$\frac{G}{Nk_BT} = -\frac{S}{Nk_B} = -\frac{N-1}{N}\ln\left(\frac{\Delta_1}{R}\right) - \frac{1}{N}\ln\left(\frac{\Delta_2(N)}{R}\right) - \frac{N-1}{N}\frac{\Delta_1}{L_0}\left(\frac{\Delta_1^2}{R_{ee}^2}\right) - \frac{\Delta_2^3(N)}{NL_0R_{ee}^2} \quad (4)$$

The first addend results from the fraction of the orientational entropy of platelets in the stack, while the second addend deals with the orientational entropy of the full stack. The solid angles have been normalized by the solid angle of a completely free clay particle. The third addend describes the product of the fraction of spaces within the stack, the number of polymers in between the platelets and the confinement entropy of the polymers. The unperturbed polymer end-to-end distance is R_{ee} (we used 57 Å for the molar mass 3350 g/mol [19]). The last addend describes the polymer confinement entropy of the polymers between the stacks.

The following conditions for the average platelet number N in the stack and the average platelet distance Δ_1 in the stack can be derived from the first derivatives ($\partial(G/N)/\partial N$ and $\partial G/\partial\Delta_1$) of the thermodynamic potential (as the minimization condition):

$$\ln\left(\frac{\Delta_1}{\Delta_2}\right) + \frac{\delta-\Delta_1}{\Delta_2} + P\left(\Delta_1^3 + \Delta_2^3\left(3\frac{\delta-\Delta_1}{\Delta_2} - 1\right)\right) = 0 \quad (5)$$

and

$$\frac{1}{\Delta_1\Delta_2} - 3P(\Delta_1+\Delta_2) = 0 \quad (6)$$

We assume that the parameter δ is given by the fraction of platelets in the sample, and $\Delta_2(N) = N\delta-(N-1)\Delta_1$ is determined implicitly. We abbreviate $P = (L_0R_{ee}^2)^{-1}$. From the second derivative of the thermodynamic potential $\partial^2G/\partial N\partial\Delta_1$ the decay length of this model is obtained, i.e.:

$$L^{-1} = (\Delta_2-\Delta_1)^2\left(\frac{1}{\Delta_1\Delta_2^2} + 3P\right) \quad (7)$$

In this way, the scattering model (Eq. (1)) can be compared to the thermodynamic model Quantitatively. For numerical reasons, it is beneficial to define dimensionless parameters as $P\delta^3$ {1}, Δ_1/δ {0.07} and δ/L {experimental} with the starting conditions given in brackets. One consequence of this model is that the stack number N varies in the range between 1 and 3–4 for large number of free polymers (P large) to a small number of free polymers (P small). A small finite stack number is also confirmed by TEM measurements [4]. That means that clay platelets in thermodynamic equilibrium with polymers do not form extremely large stacks. The enthalpic highly favorable interaction of the polymer with the clay results in a small number of free polymers (small P). Only if enthalpic interactions are highly unfavorable (not considered here) the clay platelets do not mix with the polymer.

For describing the scattering curves of the clay stacks at relatively high q, we need the form factor of the single platelets. The form factor of a clay platelet in the normal direction is usually [1] described by a layer tetrahedrons with silicon in the center and oxygen at the vertex that are connected to a layer of octahedrons with aluminum in the center and the same oxygen atoms at the vertices that once more is followed by a layer of tetrahedrons. The positions of the atoms Al/O/Si/O from the center read 0, $\sqrt{2}/3$,$\sqrt{2}/3+\sqrt{6}/4$,$\sqrt{2}/3+\sqrt{2/3}$ in relative units of a length l_0 of the order of 3.5 Å. From the approximate sum rule $Al_2Si_2O_{12}H_2$ we allocate the electron numbers according to the oxidization states of 10 to each of those atoms. Thus the x-ray form factor is:

$$F(q) = 20 + 60\cos\left(\frac{\sqrt{2}}{6}ql_0\right) + 40\cos\left(\left(\frac{\sqrt{2}}{6}+\frac{\sqrt{6}}{8}\right)ql_0\right) + 60\cos\left(\left(\frac{\sqrt{2}}{6}+\sqrt{\frac{1}{6}}\right)ql_0\right) \quad (8)$$

The prefactors 20/60/40/60 are connected to the electron numbers of the atoms, which is exchanged for the neutron scattering lengths of the atoms according to 2×3.45, 3×5.80, 2×4.15, and 3×5.80 in fm according to the NIST data table [20]. Then the overall scattering function is connected to the following expression:

$$\frac{d\Sigma}{d\Omega}(q)\ (F(q)-F_0)^2\times(\phi S(q)+1-\phi) + S_{cryst}(q) + b_{background} \quad (9)$$

Each of the factors of the form and structure is extended by a constant term due to (a) the polymer scattering that at this stage is assumed to arise from uncorrelated atoms and due to (b) the fraction (1-ϕ) of isolated platelets. The possible crystallinity appears as an incoherent superposition of the structure in terms of $S_{cryst}(q)$ and is not discussed any further in terms of a mathematical model. An additional background term is allowed for more freedom in the fitting procedure.

3. Results

The XRD patterns of the LRD-PEO nanocomposites are displayed in Fig. 1. There are several peaks identified that originate to different phenomena. The peaks indicated with A, B, and C originate from the crystalline structure of PEO at room temperature [21]. Only the liquid PEO with a molar mass of 600 g/mol does not show the peaks, and the molar mass of 1000 g/mol presents the peaks very weakly. The other peaks at smaller scattering angles originate from the presumably regular arrangement of the clay particles with intercalated polymer. Taking the 10° peak as a second order peak results in a regular spacing of roughly 18 Å. A detailed analysis is performed at a later stage further down in this manuscript.

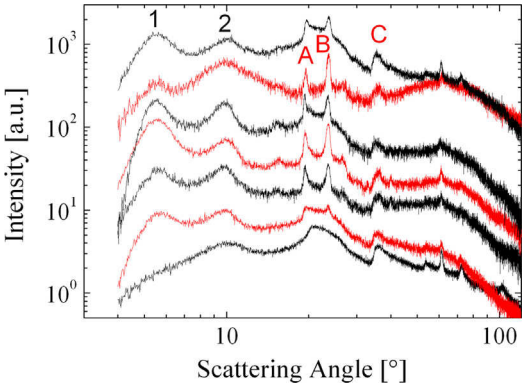

Fig. 1. X-ray diffraction images of the clay-polymer nanocomposites with varying molar masses of the polyethylene oxide polymer that were 600, 1000, 1500, 3350, 10,000, 20,000, and 100,000 from the bottom to top. All intensities are not calibrated and are shifted for better visibility. The strongly increasing intensity at lowest angles is due to the shading of the beam stop, and is corrected for the measurements presented in Fig. 3.

SANS/WANS measurements were performed on the same systems, and due to the similar XRD patterns and highly comparable SANS/WANS patterns the curves have been averaged for the polyethylene oxide molar masses of 1000, 1500, 3350, 10,000, 20,000, and 100,000 g/mol. The resulting curve is presented in Fig. 2. For background subtraction we modeled a possible curve using two different power laws as indicated by the dashed line. This method is not highly quantitative, but results in better visible peaks as we will see below. But already here we see a clear shoulder at Q = 0.3 Å^{-1} and the two strong peaks from the crystalline polyethylene oxide as indicated A, and B in Fig. 1.

In Fig. 3 we see now corrected curves (as described above). While the blue curve and the black solid line display the representative bulk case from XRD and neutron measurements, the surprising measurement is found for a LRD-PEO system with a molar mass of 3350 g/mol that resulted in a solvent cast film at the margin of the bulk sample. It obviously had a higher stack number of the clay arrays resulting in sharper peaks on the low q-side, but also more peaks at the higher q-side. Those peaks are indicated with green numbers ranging from 1 to 6, while the PEO crystals are connected to peaks A and B. The representative bulk scattering curves have only 1–2 peaks arising from the clay stacking. There are also model fits with the described model in the corresponding section above. As one sees the modeling is semi-quantitatively describing the wide-angle scattering of the clay arrangements. The exact peak positions and intensities are not extremely well covered as one expects for classical SANS models. Flaws of the model are discussed further below.

4. Discussion

In this section we like to discuss the model parameters obtained from the fitting. We start with the LRD-PEO system with a higher number of platelets in the stacks with a molar mass of 3350 (red curve). The reference electron number (that is normalized to the same volume as all clay atoms) F_0 was 7.4 that seems to be reasonable for the atoms of the ethylene oxide monomer (C_2H_4O) due to the lower density. The length parameter l_0 of the form factor was 2.6 Å that results in an approximate distance of 6.7 Å for the outer oxygen layers. Usually, there are further hydrogen atoms and counterions surrounding the clay sheets resulting in an effective thickness of 10 Å. The fraction of free platelets was approximately 10% that seems reasonably low (i.e. $\phi = 0.9$). The decay length L

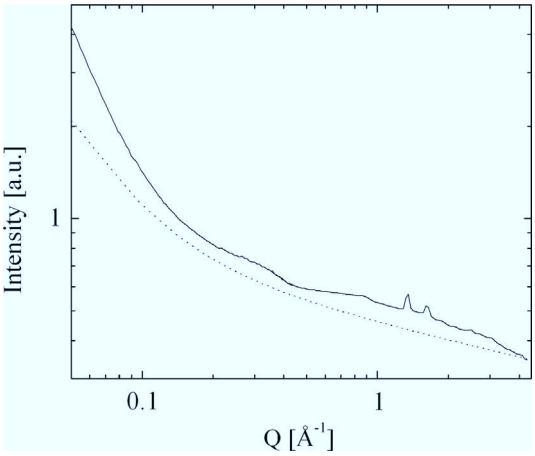

Fig. 2. SANS/WANS scattering intensities of the clay-polymer nanocomposites as averaged for the polyethylene oxide molar masses 1000, 1500, 3350, 10,000, 20,000, and 100,000 g/mol. This average was performed because the XRD measurements looked rather identical, and the single measurements had worse statistics. The dotted line indicates the background of the measurement.

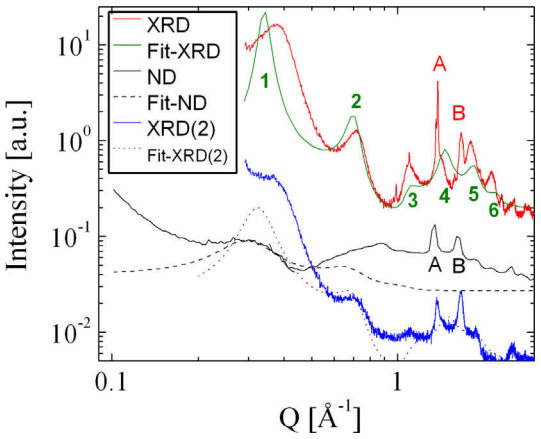

Fig. 3. Combination of XRD and SANS/WANS patterns at arbitrary intensity scale with corrections as described in the text. The red curve resulted from a dry cast film sample at the margin (with fit in green). For comparison the blue curve resulted from a bulk sample with much less pronounced peaks from the clay platelet arrangements (with fit in dotted line). However, this curve is highly representative for all polymer molar masses. The black line displays the SANS/WANS curves (with fit in dashed line). (For interpretation of the references to colour in this figure legend, the reader is referred to the web version of this article.)

was modeled to be 2.6 Å(±0.3 Å) that speaks for a rather tightly packed stack. The offset repeat distance, i.e. the repeat distance d of clay particles that cannot be further shrunk is modeled to be 16.3 Å(±0.5 Å). This number sounds reasonable for a single monomer layer of PEO monomers tightly bound to each platelet surface. In previous measurements of PEO and LRD in solution we have observed a strong binding of the two components [22,23]. The sum $L + d = 19$ Å(±0.8 Å) seems to fit the very first estimation of the second order Bragg peak position from the XRD measurements. The first order Bragg peak of the currently discussed measurement is not very well reproduced by the model, and might be an issue of the shading correction. For all model peaks, the exact peak position and the intensity are not fully covered by the model at these wide angles. While one usually expects a much better agreement for classical small-angle scattering models, the wide-angle scattering depends at this point much more on exact atom positions such that classical soft-matter approaches are a little insufficient as applied here. Furthermore the tilt of the platelets is not treated in the scattering model contrarily to the thermodynamic approach. The overall scattering function of the clay arrangement has been multiplied with a Gaussian function $\exp(-\sigma^2 q^2)$ for the atomistic finite size with $\sigma \approx 1$Å(±0.2 Å) being the right size.

The second fit curve was modeled with neutron scattering lengths instead, and mainly the decay length L was replaced by a value of 12 Å(±1Å), which connects to a much less ordered stack, while all the structural parameters stayed the same. That means that in the representative ordinary bulk there is a weaker tendency for ordering that is already seen by the smaller number of wider and less pronounced peaks of the bulk samples (see also the XRD scattering of Fig. 1 for instance). Similarly, the bulk sample of LRD with PEO polymer of the molar mass 3350 obtains a decay length of 6 Å(±0.6 Å).

The proposed structure factor (Eq. (1)) makes connection to physical magnitudes of the system and can be compared to the thermodynamic modeling of clay-polymer systems (Eq. (4) and below). The very first paracrystal model of Kratky/Porod [24–26] does not contain any thermodynamics and thus does not provide much physical insight, even though an equally good semi-quantitative agreement could be achieved as well.

Comparing the measured dacay length of the bulk and the average distance of the clay platelets $\delta = d_0/(1 - \varphi_{pol}) - d_0 = 52$ Å(±1Å)

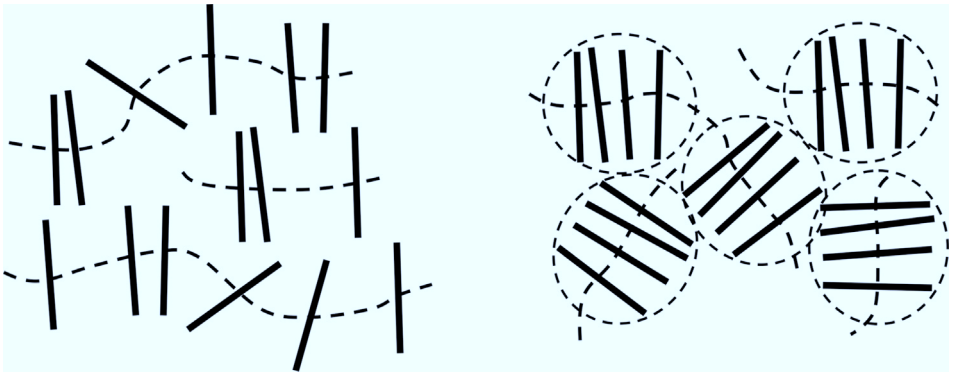

Fig. 4. Sketches for the meaning of the locally columnar model that connects a scattering model with a thermodynamic model.

with the model (Eqs. (5)–(7)), using the naked platelet thickness of d_0 = 10 Å here), we arrive at the following parameters for the thermodynamic model: Δ_1 = 13.8 Å(±1.5 Å), Δ_2 = 66 Å(±7Å), N = 1.4 (±0.1). The latter platelet number in the stack compares well to the scattering model (Eq. (3)) with N = 1.25(±0.08). Also, the average stack distance Δ_1 is in between the bare measured L = 12 Å(±1Å) and the maximum value of $L + d - d_0$ = 18 Å(±1.5 Å). From the SAXS measurements of the bulk sample, we obtain a decay length of L = 6 Å(±0.6 Å) that results in similar parameters Δ_1 = 9.0 Å(±1Å), Δ_2 = 80 Å(±8Å), N = 1.3(±0.1). While these values may possibly be more representative, the general statement stays the same. The low N values mean that only very little stacks form of mainly 2 platelets. But the presence of a correlation peak clearly indicates correlations at shorter distances than the average distance. Taking now the example of the higher degree of order (red curve in Fig. 3) with L = 2.6 Å(±0.3 Å) and leaving the polymer interaction the same, i.e. P is unchanged, we arrive at the parameters: Δ_1 = 2.6 Å(±0.3 Å), Δ_2 = 166 Å(±20 Å), N = 3.3(±0.4). Again, the bare scattering model (Eq. (3)) predicts N = 3.6(±0.5) in very good agreement. The average stack distance Δ_1 seems to approach the decay length L. The overall agreement between the bulk and marginal sample is a hint for a coexistence that bases on the same physical parameters.

The very small parameter of our modeling of $P = 4.6 \times 10^{-6}$ Å^{-3} is much smaller than from the estimation of all free polymers with P = 0.011 Å^{-3}. The arguments already arose above point towards the strong binding of the PEO polymers to the LRD platelets. That means that the confinement of the majority of polymers does not contribute to the entropy, and so only a very small fraction of polymers stays free. We assumed a parabolic monomer distribution for the free polymers that turns down to zero at the clay platelets and with a typical width connected to the free polymer size and compared that to a constant polymer density. From that, a 140 times lower polymer fraction for the free polymers is obtained that gives the right direction for the missing factor of the P values. The measured discrepancy factor of 2400 gives the experimental fraction of 1:2400 of free polymers in our system. This is the essential result of the application of our model to the scattering data. However, the small values of P explain well that a detailed dependence to the polymer size or molar mass is not given, because the tilt entropy of the clay platelets is dominating.

5. Conclusions

We developed a connection between a scattering model and a thermodynamic model that we call the "*locally columnar model*" for clay systems holding for semi-dilute and more concentrated systems. The basis is that the clay particles form locally a columnar system, i.e. stacks, that allow more freedom to the arrangement of the platelets and stacks in terms of tilt along a rather weakly defined line. These concentric stacks experience a very high entropic violation of $Nk_B\ln(2)$ for the interdigitation, which is highly unfavorable. For smaller stacks, the particles line up along rather long virtual threads (see Fig. 4 left) while there can be coexistence for thicker stacks that are quite released (see Fig. 4 right), because the stack distance Δ_2 grows larger. The scattering model goes along that concept and deals with a distance distribution arising from a chemical potential [1]. Both models make a link via that chemical potential/distance relation by the effective L parameter. For our case we found that the polymers are tightly bound to the clay particles [22,23] and that then the rotational entropy of the single platelets is dominating.

A rather similar concept was derived in Ref. [6] that starts from a rather analytical treatment of the free energy. Unfortunately, the focus did not lie on the distance distribution as in our case. Density functional theories from the same group [7–10] partially neglected the rotational freedom between neighboring platelets but considered a large number of different phases. Other attempts for connections between scattering and models exist in the literature too [13]. And also simulations are possible for not too large systems [11]. As the simplest approach, there is a coexistence between an isotropic and a nematic phase [6]. That translates within our approach to a coexistence of thin stacks that line up and thick stacks that are rather oriented randomly. In theories [6], the clay particle concentration for that coexistence region heavily depends on the platelet diameter. A more detailed analysis of that coexistence within our approach is missing.

While our thermodynamic model is still rather rudimentary it provides new insight to the connection with scattering models. In this sense, we hope for more connections to better theoretical approaches as cited above that then would give deeper insight through comparisons of (scattering) experiments with theory. Especially this connection has not been made thoroughly in the past.

Acknowledgements

We thank Helmut Coutelle from the former Rockwood section, Moosburg, for his kind provision of clay samples.

References

[1] K. Jlassi, M.M. Chehimi, S. Thomas, Clay-Polymer Nanocomposites, Elsevier, Amsterdam, 2017.
[2] D.L. Ho, R.M. Briber, C.J. Glinka, Chem. Mater. 13 (2001) 1923–1931.
[3] E. Loizou, P. Butler, L. Porcar, E. Kesselman, Y. Talmon, A. Dundigalla, G. Schmidt, Macromolecules 38 (2005) 2047–2049.
[4] V. Causin, C. Marega, A. Marigo, G. Ferrara, Polymer 46 (2005) 9533–9537.
[5] C. Marega, A. Marigo, G. Cingano, R. Zanetti, Polymer 37 (1996) 5549–5557.
[6] Y. Lyatskaya, A.C. Balazs, Macromolecules 31 (1998) 6676–6680.

[7] V.V. Ginzburg, C. Singh, A.C. Balasz, Macromolecules 33 (2000) 1089–1099.
[8] V.V. Ginzburg, A.C. Balasz, Macromolecules 32 (1999) 5681–5688.
[9] A.C. Balasz, C. Singh, E. Zhulina, Macromolecules 31 (1998) 8370–8381.
[10] A.C. Balasz, C. Singh, E. Zhulina, Y. Lyatskaya, Acc. Chem. Res. 32 (1999) 651–657.
[11] R.T. Cygan, J.A. Greathouse, H. Heinz, A.G. Kalinichev, J. Mater. Chem. 19 (2009) 2470–2481.
[12] A.G. García, H.H. Wensink, H.N.W. Lekkerkerker, R. Tuinier, 2017 arXiv: 1711.04143v1.
[13] R.A. Vaia, E.P. Giannelis, Macromolecules 30 (1997) 8000–8009.
[14] H. Frielinghaus, W. Pyckhout-Hintzen, chapter 10 neutron scattering on different states of polymer-clay compounds: from solution to dry states, in: K. Jlassi, M.M. Chehimi, S. Thomas (Eds.), Clay-Polymer Nanocomposites, Elsevier, Amsterdam, 2017.
[15] R. Hosemann, S.N. Bagchi, Direct Analysis of Diffraction by Matter, North-Holland Publishing Company, Amsterdam, 1962.
[16] T. Ishigaki, A. Hoshikawa, M. Yonemura, T. Morishima, T. Kamiyama, R. Oishi, K. Aizawa, T. Sakuma, Y. Tomota, M. Arai, M. Hayashi, K. Ebata, Y. Takano, K. Komatsuzaki, H. Asano, Y. Takano, T. Kasao, Nucl. Instr. Meth. Phys. Res. A 600 (2009) 189–191.
[17] Y. Onuki, A. Hoshikawa, S. Sato, P. Xu, T. Ishigaki, Y. Saito, H. Todoroki, M. Hayashi, J. Appl. Cryst. 49 (2016) 1579–1584.
[18] P.G. de Gennes, Macromolecules 13 (1980) 1069–1075.
[19] S. Kawaguchi, G. Imai, J. Suzuki, A. Miyahara, T. Kitano, K. Ito, Polymer 38 (1997) 2885–2891 (For small molecules, the end-to-end distance does not change between the melt and solution).
[20] <https://www.nist.gov/ncnr/neutron-scattering-lengths-list>.
[21] Y. Takahashi, H. Tadokoro, Macromolecules 6 (1973) 672–675.
[22] R.L. Parfitt, D.J. Greenland, Clay Miner. 8 (1970) 305–315.
[23] X. Frielinghaus, M. Brodeck, O. Holderer, H. Frielinghaus, Langmuir 26 (2010) 17444–17448.
[24] O. Kratky, G. Porod, J. Coll. Sci. 4 (1949) 35.
[25] R.A. Vaia, W. Liu, J. Polym. Sci. Part B: Polym. Phys. 40 (2002) 1590–1600.
[26] H.J.M. Hanley, C.D. Muzny, D.L. Ho, C.J. Glinka, Langmuir 19 (2003) 5575–5580.